Tectonophysics 468 (2009) 113–130

Contents lists available at ScienceDirect

Tectonophysics

journal homepage: www.elsevier.com/locate/tecto

Response of a multi-domain continental margin to compression: Study from seismic reflection–refraction and numerical modelling in the Tagus Abyssal Plain

M.C. Neves [a,*], P. Terrinha [b], A. Afilhado [c], M. Moulin [d], L. Matias [e], F. Rosas [d]

[a] CIMA-FCMA, Universidade do Algarve, 8000 Faro, Portugal
[b] INETI, Dep. Marine Geology, Estrada da Portela, 2721-866 Amadora, Portugal
[c] Instituto Superior de Engenharia de Lisboa, Dep. de Engenharia Civil, R. Conselheiro Emidio Navarro, 1, Portugal
[d] LATTEX-IDL, Dep. of Geology, FCUL, Campo Grande, Ed C6, Piso 2, 1749-016 Lisboa, Portugal
[e] CGUL, IDL, FCUL, Portugal

ARTICLE INFO

Article history:
Received 10 September 2007
Received in revised form 14 April 2008
Accepted 8 May 2008
Available online 17 May 2008

Keywords:
Tectonic inversion of rifted margin
Seismostratigraphy
Deep structure
FEM modelling
West Iberia Margin

ABSTRACT

The effects of the Miocene through Present compression in the Tagus Abyssal Plain are mapped using the most up to date available to scientific community multi-channel seismic reflection and refraction data. Correlation of the rift basin fault pattern with the deep crustal structure is presented along seismic line IAM-5. Four structural domains were recognized. In the oceanic realm mild deformation concentrates in Domain 1 adjacent to the Tore–Madeira Rise. Domain 2 is characterized by the absence of shortening structures, except near the ocean–continent transition (OCT), implying that Miocene deformation did not propagate into the Abyssal Plain. In Domain 3 we distinguish three sub-domains: Sub-domain 3A which coincides with the OCT, Sub-domain 3B which is a highly deformed adjacent continental segment, and Sub-domain 3C. The Miocene tectonic inversion is mainly accommodated in Domain 3 by oceanwards directed thrusting at the ocean–continent transition and continentwards on the continental slope. Domain 4 corresponds to the non-rifted continental margin where only minor extensional and shortening deformation structures are observed.

Finite element numerical models address the response of the various domains to the Miocene compression, emphasizing the long-wavelength differential vertical movements and the role of possible rheologic contrasts. The concentration of the Miocene deformation in the transitional zone (TC), which is the addition of Sub-domain 3A and part of 3B, is a result of two main factors: (1) focusing of compression in an already stressed region due to plate curvature and sediment loading; and (2) rheological weakening. We estimate that the frictional strength in the TC is reduced in 30% relative to the surrounding regions.

A model of compressive deformation propagation by means of horizontal impingement of the middle continental crust rift wedge and horizontal shearing on serpentinized mantle in the oceanic realm is presented. This model is consistent with both the geological interpretation of seismic data and the results of numerical modelling.

1. Introduction

1.1. The Tagus Abyssal Plain and the Iberia Continental Margin

It is now widely recognized that many non-volcanic rifted continental margins are characterized by the presence of a transitional zone between the thinned continental crust and oceanic crust. However, the nature of this zone is still a matter of debate and different hypotheses have been suggested for its origin in the West Iberia Margin (WIM): i) thin, tectonized oceanic crust formed at the early stages of accretion by ultra-slow spreading ridge or in a magma starved accretion setting (Sawyer, 1994; Minshull et al., 1998; Srivastava et al., 2000); ii) very thinned continental crust (Whitmarsh et al., 1990; Whitmarsh and Miles, 1995) and iii) exhumed, highly serpentinized mantle (Boillot et al., 1989; Pickup et al., 1996; Chian et al., 1999; Dean et al., 2000; Whitmarsh et al., 2001). The anomalous crust is underlain by a layer with P-wave intermediate velocities between 7.0 and 7.6 km/s in various Atlantic margins. This layer is interpreted either as serpentinized upper mantle (Boillot et al., 1989; Chian et al., 1999) or as an evidence for underplating (White and McKenzie, 1989; Kelemen and Holbrook, 1995).

The WIM and its conjugate, the Newfoundland margin (Fig. 1A) that broke apart in the Early Cretaceous (in Barremian times), are examples of margins where the ocean–continent transitional zone has been recognized and extensively investigated by geophysical methods (Mauffret et al., 1989; Pinheiro et al., 1992; Reid, 1994; Whitmarsh

* Corresponding author. Tel.: +351 289800938; fax: +351 289800069.
E-mail addresses: mcneves@ualg.pt (M.C. Neves), pedro.terrinha@ineti.pt (P. Terrinha), afilhado@dec.isel.ipl.pt (A. Afilhado), mmoulin@fc.ul.pt (M. Moulin), lmmatias@fc.ul.pt (L. Matias), frosas@fc.ul.pt (F. Rosas).

0040-1951/$ – see front matter © 2008 Elsevier B.V. All rights reserved.
doi:10.1016/j.tecto.2008.05.008

and Miles, 1995; Miles et al., 1996; Whitmarsh et al., 1996; Pickup et al., 1996; Gonzalez et al., 1999; Chian et al., 1999; Dean et al., 2000; Funck et al., 2003; Hopper et al., 2004; Lau et al., 2006a,b; Van Avendonk et al., 2006; Shillington et al., 2006; Sibuet et al., 2007; Afilhado et al., in press) and ocean deep drilling (Boillot et al., 1987; Sawyer et al., 1994; Whitmarsh et al., 1998; Tucholke et al., 2004).

To the north, the Galicia Bank and Flemish Cap form a very asymmetric pair of conjugate margins. The abrupt necking of the continental crust without tilted blocks in the Flemish Cap (Funck et al., 2003; Hopper et al., 2006) contrasts with the gradual thinning of the continental crust in Galicia, where a number of tilted blocks are recognized on top of a major detachment, the "S-reflector" (Reston et al., 1996; Whitmarsh et al., 1996). There is no evidence in Flemish Cap for the zone with serpentinized upper mantle like in the Galicia Margin (ibid.). Instead, the transitional zone in the Flemish Cap is considered to be made up mostly of oceanic crust formed by ultra-slow accretion (Hopper et al., 2006).

Further south, the Iberia Abyssal plain and its conjugate margin, the Grand Banks in Newfoundland (IAP and GBN in Fig. 1A), show a very different picture. In the Iberian side the transitional basement comprises highly thinned continental crust attached to a large zone (~150 km) of exhumed and serpentinized continental mantle on the oceanic side (Pickup et al., 1996; Dean et al., 2000). In the Newfoundland side most of the transitional basement is of continental affinity (Shillington et al., 2006; Van Avendonk et al., 2006; Lau et al., 2006a,b). Furthermore, the partial serpentinized mantle underlying the thinned continental crust, as recognized in the Iberia Abyssal plain (Chian et al., 1999; Dean et al., 2000), is not wide spread on the Newfoundland side, as normal mantle velocities are also indicated in SCREETCH2 (Van Avendonk et al., 2006).

The Tagus Abyssal Plain and its conjugate margin, the southeast Grand Banks in Newfoundland, have not been drilled and were much less investigated by geophysical methods, than the margins to the North. The interpretation and modelling of wide angle and near vertical seismic data along IAM-5 multi-channel (MCS) profile (Afilhado et al., in press) indicates that nearly the entire TAP is underlain by oceanic crust (Domains 1 and 2 in Fig. 1B). Both seismic data, magnetic and free-air modelling concur to the identification of a major rock property contrast at ~10.5°W (Domain 2/Domain 3 contact in Fig. 1B), which is interpreted as the eastern limit of the oceanic crust. Between this location and Madeira–Tore Rise, the MSC and wide angle data indicate that the oceanic crust thins almost to nought locally. This thinning can be related to the decrease of magma supply, allowing for the serpentinization of the shallowest mantle levels [ibid.], which is in good agreement with the P-wave velocities modelled by Pinheiro et al. (1992) in that area.

To the east of ~10.5°W Afilhado et al. (in press) recognised an approximately 40 km wide zone called the OCT (Fig. 2), similar to the zone of exhumed serpentinized mantle recognized in the Iberia Abyssal Plain to the north. However, the OCT in the TAP is rather narrower than the exhumed serpentinized mantle zone in the Iberia Abyssal Plain.

The southeast Grand Banks margin shows a succession of domains very similar to the conjugate margin in the TAP, but with smaller widths (Reid, 1994). Both margins show a very small number of tilted blocks. While the anomalous velocity upper mantle is recognized in the Grand Banks, no similar layer was identified in the TAP, but its presence cannot be excluded below the thinned continental crust domain (Afilhado et al., in press).

The interpretation of the geo-transect proposed by Afilhado et al. (in press) for the TAP, along the IAM-5 seismic line, is in contradiction with previous interpretations by other authors, who assimilate the whole extent of the crust at the TAP to oceanic crust (Mauffret et al., 1989; Srivastava et al., 2000) or to transitional crust (Rovere et al., 2004). Although indicating different locations for the OCT, Pinheiro et al. (1992) and Afilhado et al. (in press) both conclude that the transitional basement extends over a narrow zone in the TAP. The interpretation of the different crustal/lithosphere domains have important consequences on the proposed ages for the earliest ocean floor and for plate reconstruction models, as shown by the difficulties of closing the conjugate margins using only the unquestionable domains of conjugate continental crust (Klitgord and Schouten 1986; Olivet, 1996, Srivastava et al., 2000; Sibuet et al., 2004).

The WIM was subjected to the remote effects of the main Late Cretaceous through Miocene orogenesis that led to the formation of the Pyrenees and the Betics, associated with the east–west trending northern and southern Iberia collision boundaries, respectively. The onshore approximately east to west trending thrusts of the inverted Lusitanian rift Basin formed during Late Cretaceous, Paleogene and Miocene times (Ribeiro et al., 1990; Kullberg et al., 2000, 2006) and thrust tectonics in the south Portuguese margin and Algarve Basin occurred mostly during the Late Cretaceous and Paleogene (Terrinha, 1998; Roque, 2007). Compressive structures in the offshore were also mapped by Wilson et al. (1996) in the Iberia Abyssal Plain and by Mauffret et al. (1989) in the Tagus Abyssal Plain.

Post-rift tectonics in the shelf and upper slope that borders the TAP to the east is mostly expressed by vertical movements and erosional unconformities (Alves et al., 2003). Along IAM-5 line, reverse faulting in the Miocene seems to be concentrated at the limits of the main crustal domains (Afilhado et al., in press). Zones displaying compressional deformation of Eocene and Miocene age were also identified in the Iberia Abyssal Plain, coincident with the ocean–continent transition (Masson et al., 1994). The concentration of deformation was postulated to occur due to a rheological contrast, but no modelling supported this conclusion (ibid.). The effects of the Miocene compressive events in the TAP are fairly evident and their breadth should be evaluated and taken into account when attempting to understand the processes of formation of the margin in this area. Furthermore, rheological contrasts between crustal and mantle domains in the margin and their discontinuous geometries are likely to control the loci, style and amount of ductile deformation and faulting. In this case, rheological numerical modelling of the Miocene compressive event and the comparison of model predictions with geological observations provide additional insights into the debatable nature and geometry of the TAP's crust.

1.2. Objectives

The main goals of this paper were to see in detail, *firstly*, how do the tectonic structures observed within the sediments and shallow acoustic basement correlate with the deep structure computed from wide angle by Afilhado et al. (in press); *secondly*, how did the Miocene compression propagate across the various rheological domains of the WIM and TAP; *thirdly*, explore the comparison between the presented tectonostratigraphic model and the numerical models to investigate the interplay between Miocene compression and rheology. These goals were pursued by thoroughly studying the tectonostratigraphy of the region that encompasses the TAP and a multi-channel seismic profile (MCS) perpendicular to the WIM and TAP, the IAM-5 profile (Fig. 1B).

2. Tectonics of the Tagus Abyssal Plain

Here we present the results of the interpretation of the MCS profiles shown in Fig. 1B that allowed the production of a tectonic map and subsequent interpretation of the morphotectonics of the TAP and neighbour WIM with special detail for the Miocene through Present times.

The stratigraphic calibration of MCS IAM-5 and of all the lines shown in Fig. 1B was taken from Roque (2007). The departure point for calibration was the foot-wall of the Marquês de Pombal Fault on MCS AR92-10, and then various paths and tie-lines were checked

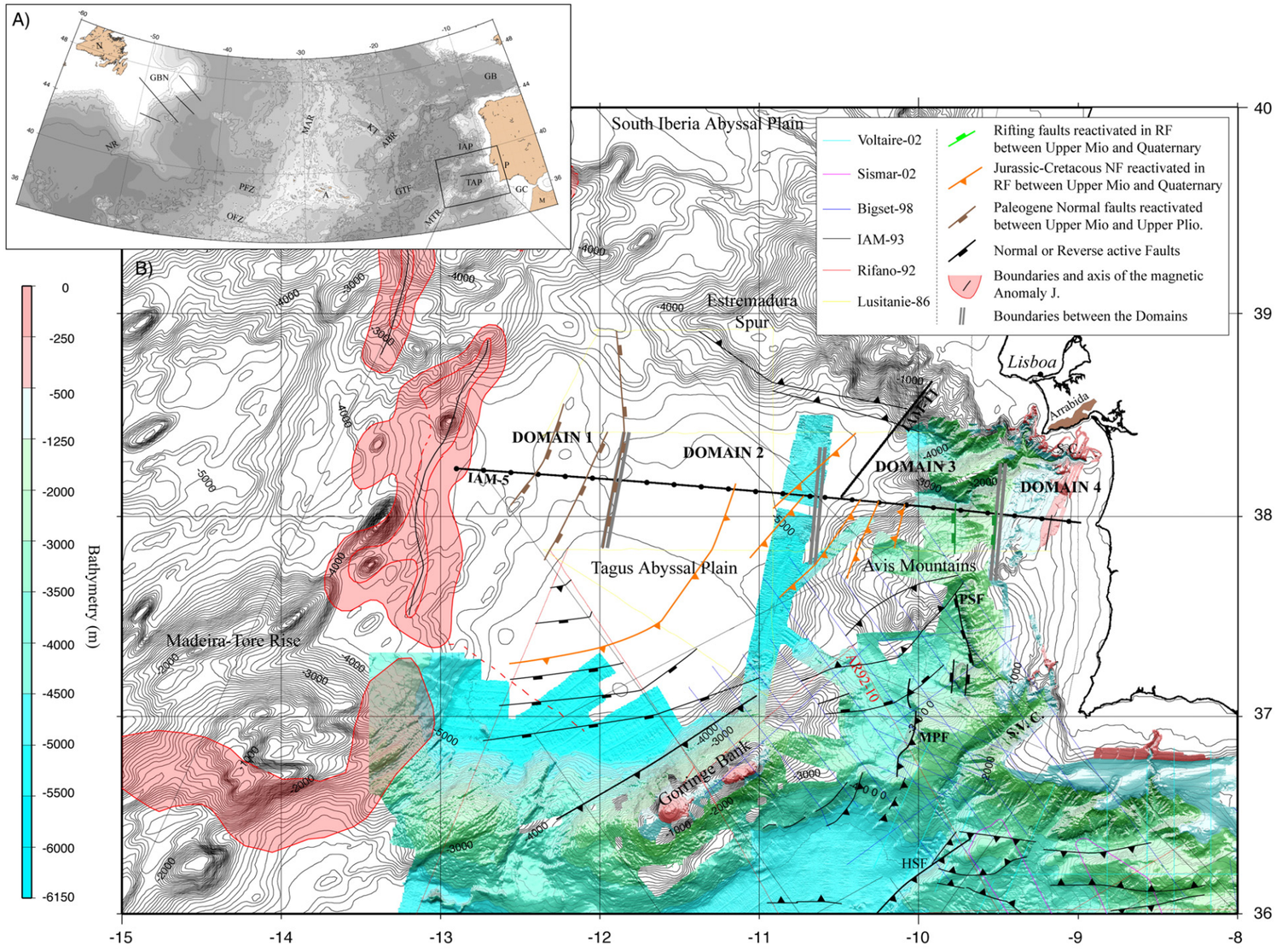

Fig. 1. A) Bathymetric map of the North Atlantic Ocean (data from Gebco97) with location of the study area including the main MCS lines. Locations of MCS lines on the homologous Grand Banks of Newfoundland margin are also shown. MAR: Mid-Atlantic Ridge; KT: King's Trough; GB: Gulf of Biscay; IAP: Iberia Abyssal Plain; TAP: Tagus Abyssal Plain; GC: Gulf of Cadiz; M: Morocco; P: Portugal; A: Azores; N: Newfoundland; GBN: Grand Banks of Newfoundland; GTF: Gloria Transform Fault, PFZ: Pico Fracture Zone; OFZ: Oceanographer Fracture Zone; ABR: Azores–Biscay Rise; MTR: Madeira–Tore Rise; NR: Newfoundland Rise. B) Tectonic–bathymetric map of the study area. Contours are every 100m (data from GEBCO97 — Digital Atlas Web Site: www.nbi.ac.uk, and Sideline et al., pers. comm.). Also shown the location of MCS lines acquired during LUSITANIE86 (Mauffret et al., 1989), RIFANO92 (Sartori et al., 1994), IAM93 (Banda et al., 1995), BIGSETS98 (Zitellini et al., 2001), SISMAR02 (Contrucci et al., 2004) and VOLTAIRE02 (Zitellini et al., 2002) surveys. Heavy lines represent the portions of the MCS lines shown in Figs. 2 and 5. The colored faults have been mapped during the present work, the black ones come from Terrinha et al. (submitted for publication). The boundaries and axis of the J Anomaly are based on the interpretation of the magnetic grid of Verhoef et al., 1996 (Fidalgo, pers. comm.). MPF: Marques Pombal Fault; SVC: Sao Vicente Canyon; SC: Setubal Canyon; HSF: Horseshoe Fault.

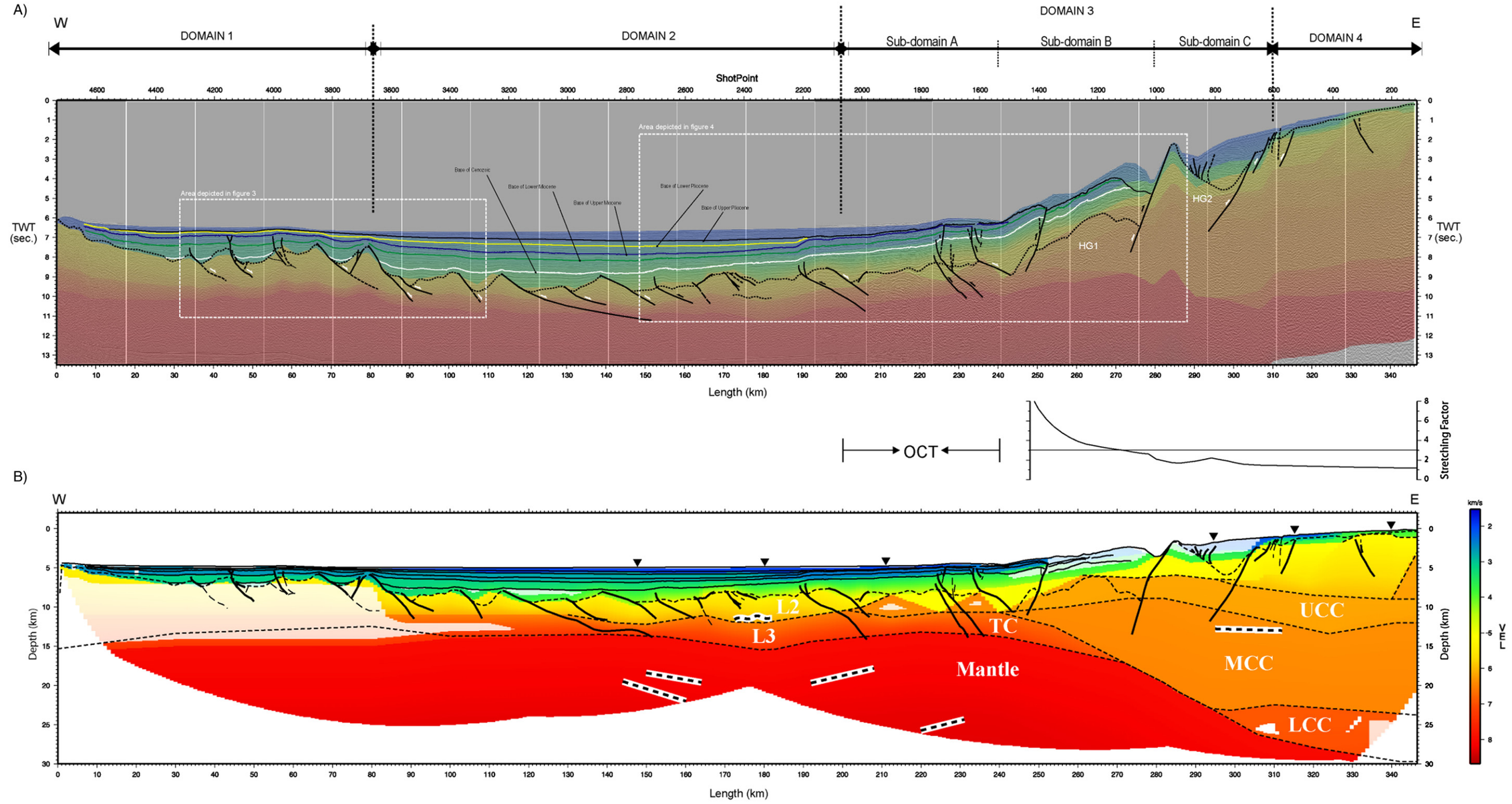

Fig. 2. A. General tectonic and seismostratigraphic interpretation of the IAM-5 MCS profile. Seismostratigraphic calibration based on Roque (2007). *White arrows*, normal fault kinematics (Late Mesozoic/Paleogene); *Black arrows*, reverse fault reactivation (ranging from Late Paleogene/Early Miocene through Present). B. Depth converted IAM-5 MCS profile with seismostratigraphic interpretation superimposed on velocity model (upper right: stretching factor of continental crust). Velocities and rheology from seismic refraction model (see text). L2 — oceanic crust layer 2; L3 — oceanic crust layer 3; UCC — upper continental crust; MCC — middle continental crust; LCC — lower continental crust; TC — transitional crust. Top and bottom velocities in km/s. The pale colors at the west end represent regions where the seismic velocity is not well resolved.

until the final stratigraphic model was obtained for IAM-5 and the TAP. The seismostratigraphic horizons taken from Roque (2007) were (Fig. 2A): i) base of Paleogene, ii) base of Lower Miocene, iii) base of Upper Miocene, iv) base of Lower Pliocene and v) base of Upper Pliocene.

The TAP displays a trapezoidal shape bound by the Estremadura Spur in the north, the TMR in the west, the Gorringe Bank in the south and the Avis Mountains in the east. The nature of these boundaries and their tectonic control are now described.

2.1. The Tagus Abyssal Plain–Tore–Madeira Rise boundary

The western limit of the TAP displays an abrupt transition from a deep seated basin filled up with more than 3 s TWT of sediments, ranging from Lower Cretaceous age through Present in the central part of the TAP, and a less than 2 s TWT thick basin in which Lower Cretaceous sediments are missing or condensed in the west.

In the acoustic basement above the Moho this transition was accommodated by means of a set of eastwards dipping extensional faults bounding rotated blocks (Fig. 2A and B) that separate a western foot-wall zone with normal thickness oceanic crust from an eastern region with thinned oceanic crust, respectively Domain 1 and Domain 2 in IAM-5 (Figs. 1B and 2). The latter is overlain by the thickest part of the deep basin that contacts abruptly with the shallower basin of Domain 1 across a N–S trending extensional fault whose main activity occurred during the Upper Cretaceous and Paleogene.

2.2. The Tagus Abyssal Plain–Gorringe Bank boundary

To the south of the TAP the seafloor rises from depth of −5000 m to a maximum of −25 m over a distance of approximately 25 km, i.e. a mean slope of approximately 11°. The slope cuts across the northwestwards directed Gorringe thrust (Fig. 1B), across which the oceanic lithosphere overthrusts sediments ranging from the Albian through Late Miocene age (Ryan et al., 1973; Auzende et al., 1978; Zitellini et al., 2004). The thrust probably initiated its activity in Early Miocene times although its main activity occurred during Mid-Late Miocene times when an olistostrome wedge was deposited at the foot of the thrust.

2.3. The Tagus Abyssal Plain–Príncipes de Avis Mountains boundary

To the east, the TAP boundary comprehends the continental slope of the West Iberian Margin that underwent the Triassic–Lower Cretaceous rifting. The submarine mountains of the Príncipes de Avis (Fig. 1B) correspond to fold and thrust structures formed during the Miocene tectonic inversion of the rifted margin. Most of the tectonic inversion structures are rooted in Mesozoic age extensional faults, which were inverted and propagated upwards forming blind thrusts that generated folds in the sedimentary cover, as can also be seen in Domain 3 in IAM-5 (Fig. 3). The main reverse faults trend NE–SW and dip towards the continent near the OCT and they reverse their thrusting polarity upslope towards the continent. The NE–SW trending segment of the Setúbal canyon sits on the submarine continuation of the southeastwards directed Arrabida thrust belt. The upper part of the continental slope at −1500 m and −970 m water depths display well preserved half-grabens bound by N–S trending faults dipping to the west. These faults show little evidence of tectonic inversion.

Shortening deformation structures of Pliocene–Quaternary age formed as reactivations of Miocene reverse faults.

2.4. The Tagus Abyssal Plain–Estremadura Spur boundary

The Estremadura Spur is an E–W trending morphological high that results from the Miocene tectonic inversion of pre-existent rift faults. On MCS profile IAM-T1 (Figs. 1B and 4) a northwards steeply dipping fault bounds a less deformed foot-wall basin. Although the sedimentary rift wedges can be observed in this MCS profile the orientation of the faults that controlled the precursor rift basin of the Estremadura Spur are still not understood due to lack of seismic data in this area. Onshore, extensional faults trending NW–SE of Middle Jurassic age in the Arrábida fold belt were reactivated as transpressional dextral strike-slip faults also common within the onshore southern part of

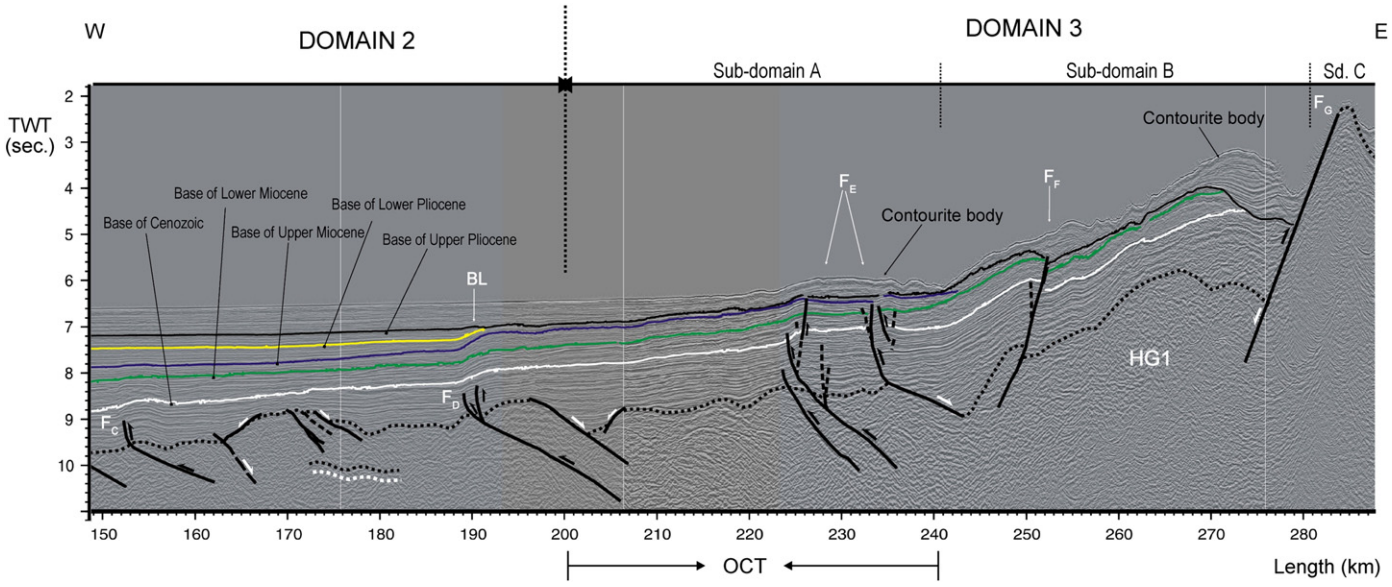

Fig. 3. Detailed tectonic interpretation of an eastern segment of IAM-5 MCS profile (zoomed from Fig. 2A). *White arrows* correspond to pre-Cenozoic normal fault kinematics (F_G is a syn-rifting normal fault which underwent Miocene reverse fault reactivation). *Black arrows* correspond to the reverse fault reactivation event with an age interval ranging from Paleogene through Late Pliocene/Present; F_C is sealed by the Early Miocene, F_D is sealed by the reflector corresponding to the base of the Upper Pliocene and, F_F affects the base of the Upper Pliocene and seemingly denotes a bathymetric expression suggesting active deformation at Present. Note that such age span denotes a diachronic migration pattern characterized by a progressively younger reverse fault reactivation towards the continental margin (i.e. towards the East). *Black and white double dashed lines* — Shallow basement reflectors. OCT — Ocean–continent transition. B — Westward migrated basin boundary (see text for further explanation).

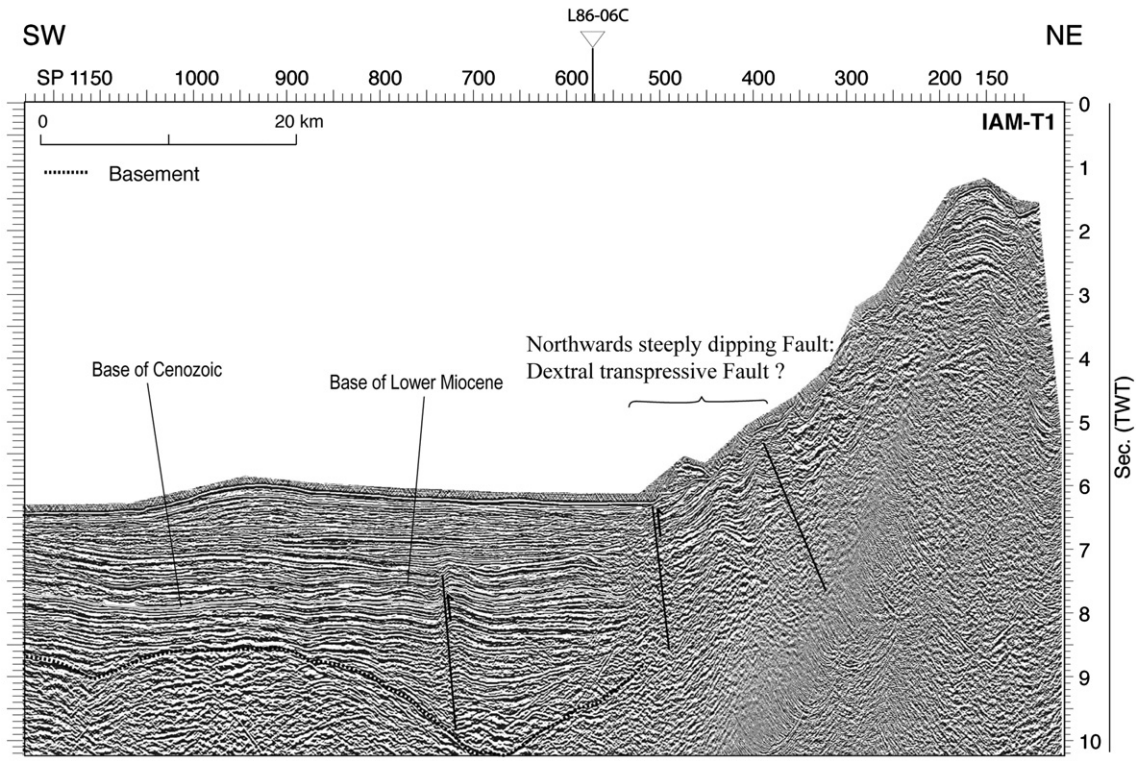

Fig. 4. General tectonic interpretation of the IAM-T1 MCS profile. The two seismostratigraphic horizons are based on the calibration of the IAM-5 profile (see Fig. 2). *Black arrows* correspond to reverse faults events. This profile illustrates the two eastern faults which can correspond to a dextral transpressive fault (see more detail in the text).

this spur (Kullberg et al., 2000, 2006). Thus, it is considered that the fault shown in Fig. 4 is a dextral transpressive fault.

3. Tectonics of line IAM-5

The MSC IAM-5 profile was analyzed in terms of its deep crustal structure and of the Meso-Cenozoic tectonic deformation. This joint analysis led to the recognition of four main structural domains (Domains 1, 2, 3 and 4), and three sub-domains (Sub-domains 3A, 3B and 3C), which are next described.

3.1. Deep crustal structure

The main rheological properties of the lithosphere along the transect MCS IAM-5 were constrained by refraction data and described in detail by Afilhado et al. (in press). Their velocity model was used to perform the depth conversion (Fig. 2B) of the interpretation of the MCS data (Fig. 2A). Based on Fig. 2A and B we next present the most relevant features concerning the crystalline crust.

3.1.1. Domain 1 and Domain 2 (the oceanic realm)

Unquestionable oceanic crust is evidenced by two high velocity gradient layers west of km200 (L2 and L3 in Fig. 2B). The basement faulted-blocks (Fig. 2A) are restricted to the upper layer L2 and the faults root at the L2/L3 level (Fig. 2B). An exception occurs at ~km150, where a listric fault roots at the Moho level. Two distinct crustal segments are distinguished to the east and west of this point (km150). In the western segment the crystalline crust is ~1–2 km thinner and the Moho ~0.5–1 km shallower than in the eastern segment (Fig. 2B).

3.1.2. Sub-domain 3A and Sub-domain 3B (the transitional region)

Sub-domains 3A and 3B are characterized by both vertical and horizontal variations of the P-wave velocity and are the most heterogeneous and interesting regions of this study. Sub-domain 3A coincides with the ocean–continent transition (OCT), having a basement velocity structure that is not oceanic or continental. Steeply dipping reflections at the base of this crustal sub-domain may be related to intrusions also suggested to occur further south (Mauffret et al., 1989). This sub-domain is also characterized by a somewhat higher density and remnant magnetization (Pinheiro, 1994; Afilhado et al., in press). Another important remark is that the faults in the OCT (F_D and F_E in Fig. 3) cross-cut the whole basement down to the Moho level (Fig. 2B). In the OCT the Moho reaches its shallowest point at km220.

The shallowest levels of Sub-domain 3B are believed to consist of middle grade metamorphosed continental crust, based on the crustal velocities and adjacent onshore geology. The crystalline crust reaches a minimum thickness of ~3 km at ~km245, underneath a thick syn-rift and post-rift sedimentary cover (Fig. 2A). However, the deepest crustal layer in Sub-domain 3B is disrupted and consequently its continental origin is uncertain. It is also in Sub-domain 3B that the stretching factor reaches a value of ~3 (at ~km270) increasing rapidly to the west of this point.

Among the 3 hypotheses for the OCT lithology, namely (i) thinned continental, (ii) slow-spreading oceanic crust, or (iii) exhumed and altered mantle, Afilhado et al. (in press) prefer a continental affinity in the upper crystalline crust, overlying a heterogeneous layer of intruded gabbros or intruded serpentinized peridotites, that extends to the east and vanishes below the unquestionable continental crust in domain 3B. We will describe later how the different hypotheses for these regions, OCT and Sub-domain 3B, were tested with the numerical modeling.

3.1.3. Sub-domain 3C and Domain 4 (the continental realm)

Unquestionable continental crust is present in Sub-domain 3C and in Domain 4. In Sub-domain 3C we note the pinch-out of the lower continental crust (LCC in Fig. 2B) at km295 implying that the middle continental crust rests directly on top of the mantle and the Moho slope reaches its maximum value (~24%). In Domain 4 the crystalline crust is ~30 km thick and the stretching factor of the continental crust is ~1.2 to 1.5 (Fig. 2B).

3.2. Seismostratigraphy

3.2.1. Domain 1

Domain 1 lies between the well developed reliefs of the TMR to the west, and the flattest area of the TAP (domain 2 to the east). Clearly localized on oceanic lithosphere this domain is characterized by important relief of the acoustic basement, comprehending several regularly spaced (~10 km) peaks overlain by a pile of sediments ranging from Upper Cretaceous through Present (Fig. 5). The height difference between positive and negative reliefs can exceed 2 km (1 s TWT) and various faults were recognized and mapped associated to these morphologies (see Figs. 1B, 2 and 5). These faults affect the basement and appear to root at the level of a strong reflective horizon at approximately 9 s TWT. This horizon is discontinuous and not imaged underneath the basement peaks (Figs. 2 and 5).

The faults in this domain strike N–S and formed during tectonic extension of Domain 1 from Cretaceous through Paleogene times and this deformation style is clearly sealed by the Lower Miocene unconformity (Fig. 5). The Upper Miocene through Lower Pliocene sedimentary packages lack any kind of extensional structures and show some mild evidences of shortening, accommodated by folding and local inversion of normal faults, but there are no well developed thrusts. Although the reverse faults do not breach out the Upper Miocene, the existence of angular unconformities and their geometry within the Upper Miocene and Lower Pliocene clearly attest for the occurrence of compressive tectonic events and associated uplift of these ages.

The kinematics of the deformation structures contemporaneous with deposition of the Lower–Middle Miocene are dubious, suggesting mild extension and shortening which can be interpreted as the result of dominant wrenching kinematics along these faults, possible associated with low angle transpression/transtension, as an effect of the NNW–SSE oriented Miocene compression in the WIM. (*cf.* F_A in Fig. 5).

Towards the western end of IAM-5, where the TMR topography is more vigorous, an increase of Pliocene–Quaternary tectonic deformation is observed, suggesting reactivation or neo-formation of reverse faults and uplift of the TMR (*cf.* Figs. 1 and 2A).

Domain 1 contacts with Domain 2 across an extensional fault formed in the Cretaceous as shown by the seismostratigraphic interpretation (Fig. 5) and active until the Early Miocene. It is parallel to the extensional faults mapped in Domain 1 and also roots within the oceanic crust at the well imaged reflector located deeper at around 10 s TWT, which also corresponds on the refraction model to the boundary between L2/L3 (Fig. 2B).

3.2.2. Domain 2

Domain 2 corresponds to the flattest area of the TAP where present-day tectonic activity is not detected in seismic reflection. Rift faults of Cretaceous age bound the main reliefs of the acoustic basement (Figs. 2A and 3). The relief of the basement of the westernmost part of this domain is identical to Domain 1; in the central and eastern parts of this domain, which coincides with the proposed OCT (Afilhado et al., in press) this relief is shallower and smoother. A NE–SW trending localized compressive structure of Paleogene age is observed (*cf.* F_C in Fig. 3) but the most important tectonic inversion structure is of Late Miocene age (*cf.* F_D in Fig. 3). This reverse fault is localized above the OCT location as proposed by Afilhado et al. (in press), showing a total vertical movement of approximately 0.58 s TWT, most of which occurred between the Late Miocene and the Late Pliocene. During this time interval, this tectonic uplift was responsible for the westwards shifting of the eastern boundary of the TAP, from km225 to km190 (BL in Fig. 3).

3.2.3. Domain 3

Domain 3 corresponds to the continental rise segment of the margin, from depths of around −4800 m to −1000 m (km200 to km310, Fig. 2A). The basement shows a series of extensional structures of Cretaceous and Late Jurassic age. Tectonic inversion of these rift faults from Early Miocene through Late Miocene accommodated most of the shortening. The Pliocene through Present compressive structures occur in this Domain upslope with respect to the most important ones of Miocene age, which concentrate in the western, more stretched and deepest part of the Domain. Domain 3 is sub-divided in three sub-domains, with different tectonic deformation, seismic stratigraphy and present-day morphology. *Sub-domain A*, from km200 to km240 (Fig. 3), displays an undulated relief. This seafloor relief results from a complex inter-action of a sedimentary deposit with a lobe shape that has been affected by

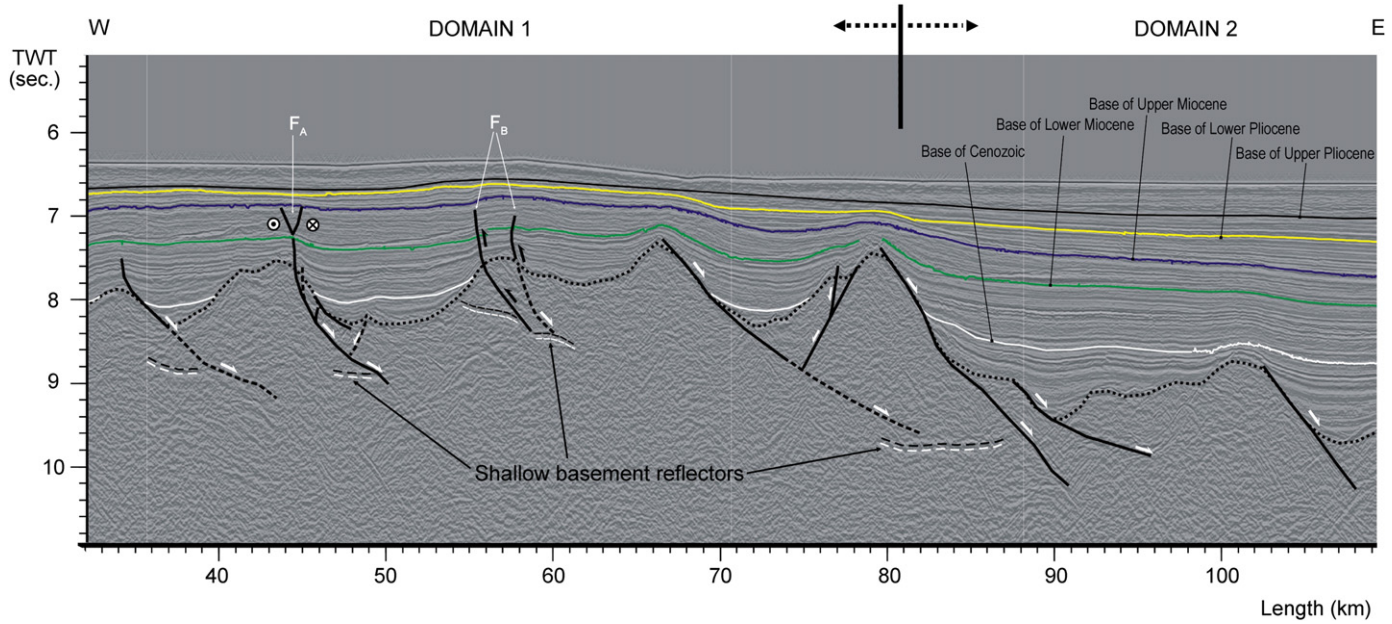

Fig. 5. Detailed tectonic interpretation of the westernmost segment of IAM-5 MCS profile (zoomed from Fig. 2A). *White arrows* correspond to normal fault kinematics through Cretaceous to Paleogene (note that this extensional event is generally sealed by the Lower Miocene); *Black arrows* correspond to the localized reverse fault reactivation event (FB) (note that this event, although mildly affecting the Upper Miocene, is sealed by the reflector corresponding to the base of the Lower Pliocene); *Crossed arrows* indicate possible left-lateral wrenching on FA faults during Early–Middle Miocene; *Black and white double dashed lines* correspond to shallow basement reflectors.

post-Late Pliocene compressive deformation and erosion. The base of the lobe, which was interpreted as corresponding to the Base of Late Pliocene horizon, lies unconformably on top of folded and faulted Lower and Middle Miocene. The Upper Miocene through Lower Pliocene hiatus is a non-deposition one caused by the westwards shift of the Domain 2 abyssal basin, as described above. The lobular sedimentary body is interpreted as having been deposited by transport at high angle to the IAM-5, i.e. either a contourite body or a mass transport deposit. *Sub-domain B* extends from km240 to km280 (Figs. 2A and 3), from water depths of −4800 m to −2400 m. The sea floor morphology and the post-Upper Pliocene sedimentary package are both irregular and affected by the eastwards directed thrusting (*cf.* F_F in Fig. 3). The most important structure in this sub-domain is the half-graben (HG1 in Fig. 2A) limited by a westerly dipping normal fault (*cf.* F_G in Fig. 3). First tectonic inversion of this half-graben occurred during Miocene times, possibly initiated in the Early Miocene. An outstanding sigmoidal superficial sedimentary body lies on top of an erosion unconformity of Late Pliocene age cutting down from the Lower Miocene through the Upper Cretaceous that are deformed by inversion of the Mesozoic rift fault (*cf.* F_G in Fig. 3). This body is interpreted in this paper as a contourite drift deposited by the Mediterranean Outflow Water between −3000 and −2300 m water depths. *Sub-domain C* extends from km280 to km310, from water depths of −2000 m to −350 m and comprehends a mildly inverted half-graben of Jurassic–Cretaceous age (HG2 in Fig. 2A).

3.2.4. Domain 4

Domain 4 extends from −350 m water depth to −150 m water depths. Stratigraphic correlation with the deeper domains shows a major unconformity of probable early Late Miocene age sealing compressive deformation folds. The top sedimentary wedge probably contains sediments of Upper Miocene through Present. The edge of the shelf coincides with a compressive structure of uncertain Late Miocene through Present age. The top of the basement is not clearly imaged but it can be argued that it lies probably between 2.5 and 3 s TWT after some strong reflectors lying at this depth.

4. Numerical modelling

4.1. Modelling technique

We used a two-dimensional finite element program which is a modified version of the FEVPLIB package (Bott, 1997). It incorporates viscoelastic and elasto-plastic deformation with a finite yield strength using the viscoplastic method (Owen and Hinton, 1980) and has been used to model stress and displacements produced by anomalous density in a variety of tectonic settings (e.g. Bott, 1999; Zhang and Bott, 2000; Neves et al., 2004). The yield strength is computed at each depth assuming brittle and power-law creep deformation depending on temperature and composition. The condition for plastic yielding obeys the Mohr-Coulomb criterion.

The models represent a 600 km long and 140 km deep vertical section of the lithosphere. Quadrilateral elements with eight nodes form a regular grid with maximum resolution of 1 km × 0.5 km in the topmost 30 km. The plane strain hypothesis, suitable to study flexure in two-dimensions, is assumed. Gravitational body forces are generated by anomalous densities referenced to a standard density–depth profile. The standard lithostatic profile was chosen to represent undisturbed oceanic lithosphere at the western edge of the model. It comprises two layers: normal oceanic crust 6 km thick and uniform mantle below, with densities of 2850 and 3300 kg m^{-3}, respectively. The surface of the model is initially assumed to be at zero depth throughout. The development of topography is the flexural isostatic response of the model to the gravitational body forces.

In models involving flexure we need to include isostatic boundary conditions representing isostatic restoring forces. They are equivalent to the hydrostatic restoring forces caused by the effective replacement of mantle rock by material of smaller density when the surface of the elastic plate is deflected downwards (Turcotte and Schubert, 2002, page 121). The isostatic boundary conditions are proportional to the vertical displacement and the density change across each interface.

Free boundary conditions at the base of the model represent an inviscid underlying asthenosphere. The west edge of the model represents undisturbed oceanic lithosphere. The nodes down this edge are constrained to zero horizontal displacement but are free to suffer vertical displacement. The east edge of the model represents undisturbed continental lithosphere. This edge is free to move both horizontally and vertically, except when shortening is considered, in which case horizontal displacements are imposed only.

The Miocene shortening is modelled by applying successive increments of horizontal displacement to the east edge nodes. Finite deformation is allowed by a standard method for geometric non-linearity. At each stage of modelling the stiffness matrix is updated to take into account the new rheology and geometry.

4.2. Modelling procedure

Regional deformation is simulated in three stages using the finite deformation approach: stage 1, development of long-wavelength topography caused by rifting; stage 2, subsidence and flexure of the basin due to sediment loading and; stage 3, subsequent deformation due to Miocene shortening.

4.2.1. Stage 1: basin geometry at the end of rifting

The strength of the lithosphere after rifting is generally negligible, so we assume that at this time the basin is in local isostatic equilibrium. This kind of equilibrium is reproduced using a viscoleastic model driven by gravitational body forces. The relevant gravitational body forces at this stage are due to the density contrasts caused by continental stretching.

The density contrasts are obtained by subtracting the reference depth–density profile from the density structure along IAM-5 (Fig. 6). Down to approximately 30 km depth the density structure was constrained by seismic reflection and refraction data and determined by modelling the gravity anomaly (Afilhado et al., in press). Below 30 km depth we assumed a uniform mantle density of 3300 kg m^{-3} and neglected density variations related to temperature since these do not significantly affect the modelling results. Seawater and post-Miocene sediments were removed and all density interfaces lying underneath were shifted upwards, so that the top of the Miocene in the sedimentary basin was at the surface of the finite element model.

Negative density anomalies generate buoyancy forces and uplift, while positive anomalies generate downward forces and subsidence. The buoyancy of the continental crust relative to the oceanic crust/mantle will generate uplift of the continental margin (at the east end of the model) relative to the ocean basin (at the west end of the model).

4.2.2. Stage 2: subsidence and flexure due to sediment loading

Flexural compensation of the sediment load is simulated using an elasto-plastic model. Since the scope of this study is not the evolution of the margin prior to Miocene times we took a snapshot of the effect of sediment loading at the onset of the Miocene considering an elastic thickness that reflects the long-term mechanical strength of the lithosphere at that time. This means that we apply the sediment loading instantaneously and neglect strength variations during sediment loading. The sediment load is incorporated through gravitational body forces that generate downward flexure. In this case the density anomalies are not relative to the reference depth–density profile. They are positive and equal to 1270 kg m^{-3} and simulate the effective load created by the replacement of seawater (ρ_w = 1030 kg m^{-3}) by sediments (ρ_s = 2300 kg m^{-3}).

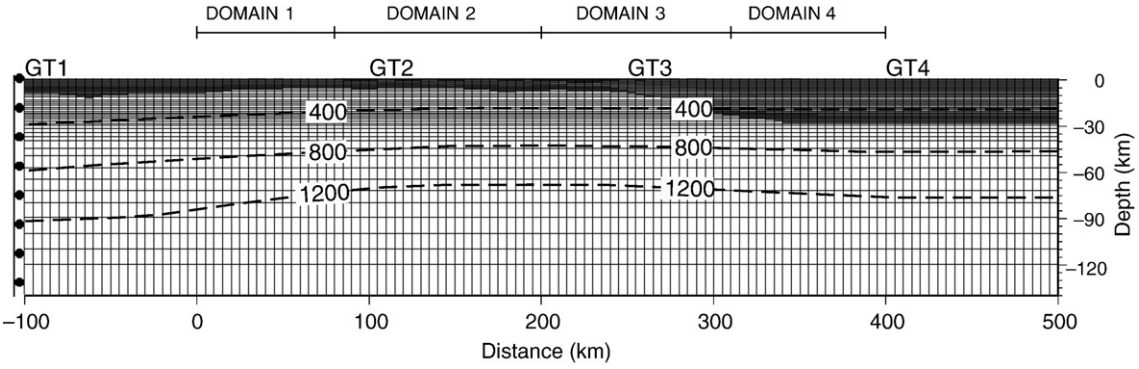

Fig. 6. Mechanical and thermal setup of the model shown with the finite element grid. The left edge is fixed in the horizontal direction and allowed to move vertically. Horizontal displacements are applied at the right edge to simulate Miocene shortening. GT1 to GT4 indicate the location of the geotherms used to build the temperature structure. Black dashed lines indicate the 400, 800 and 1200 °C isotherms. Crustal structure and densities are taken from the seismic velocity and gravity modelling, but post-Miocene sediments have been removed and all interfaces restored.

4.2.3. Stage 3: the Miocene shortening

We model the Miocene horizontal load by horizontally fixing the west edge of the model and applying successive increments of shortening to the east end. These boundary conditions imply that the edges of the model cannot rotate in a vertical plane, and thus the flexure profile must be horizontal at the edges of the model. This is not a problem because shortening sharpens the flexural bending away from the edges of the model.

In the present numerical models the total applied shortening is limited to 2000 m, in order to avoid unrealistic bending and yielding. A total of 2000 m of shortening distributed over 600 km (the length of the model) gives ~0.3% of strain. The present-day strain rate offshore SW Iberia is estimated to be about 10^{-16} s^{-1} (Jiménez-Munt et al., 2001; Negredo et al., 2002; Buforn et al., 2004). Extrapolating a strain rate in the range of 10^{-17} s^{-1}–10^{-15} s^{-1} over the past 20 Ma (since compression began) we find that an average strain of ~0.3% is a reasonable upper limit value to admit.

4.3. Rheologic assumptions

In the brittle regime the critical stress difference at failure (the yield strength) is given by the Coulomb frictional law, assuming faults of favorable orientation and negligible cohesion (Sibson, 1974),

$$\sigma_1 - \sigma_3 = \alpha \rho g z (1-\lambda) \quad (1)$$

where $\sigma_1 - \sigma_3$ is the maximum stress difference, α is a constant related to the faulting regime and frictional coefficient, ρ is the average density of rocks above depth z, and λ is the pore fluid factor. In the absence of information regarding the pore fluid factor we assume hydrostatic conditions (λ=0.4). A friction coefficient of 0.75 common to most rock types gives α=3.0 in compression (thrust faulting) and α=0.75 in extension (normal faulting).

In the ductile regime, deformation is assumed to be governed by a power-law dislocation creep equation (Ranalli, 1995),

$$\sigma_1 - \sigma_3 = \left(\frac{\dot{\varepsilon}}{B}\right)^{\frac{1}{n}} \exp\left(\frac{A}{nRT}\right) \quad (2)$$

where $\dot{\varepsilon}$ is the strain rate (s^{-1}), R is the Universal gas constant, T is the absolute temperature, A is the creep activation enthalpy and B and n are material creep parameters. The yield strength envelope is build assuming that at each depth the maximum stress difference is given by the minimum of Eqs. (1) and (2). A bulk strain rate of 10^{-16} s^{-1} is assumed.

Given the lack of surface heat flow measurements in the TAP we build a simple temperature structure by fixing 4 geotherms (GT1 to GT4 in Fig. 6) and linearly interpolating between them. GT1 is the asymptotic geotherm for oceanic lithosphere 100 Ma old (~20 Ma before present), computed according to the plate cooling model (plate thickness = 100 km). GT2 to GT4 are computed by solving the steady state 1-D heat conduction equation with radiogenic heat production for three-layer lithospheric models of varying thickness and composition. A continental surface heat flow of 61 mW m^{-2} (Fernandez et al., 1998) and a surface temperature of 15 °C is assumed. Further south, Fernandez et al. (2004) used a finite element code that solves simultaneously the geopotential, lithostatic, and heat transport equations to model the temperature structure along a profile across Cape St. Vincent. Our thermal model is similar to their results, with smoothly varying geotherms not very affected by the crustal thickness variations along the continental margin. Furthermore, models offshore Cape St. Vincent showed that the deformation in the OCT is not very sensitive to plausible temperature gradients (Neves and Neves, submitted for publication).

The compositional structure along the profile was derived from the density model and the seismic refraction data, following studies that correlate seismic velocities measured in the laboratory and dominant lithology (e.g. Christensen and Mooney, 1995; Okaya et al., 1996). In the oceanic crust, geological and geophysical observations support the choice of a dry diabase rheology (Escartín et al., 1997). In the continental crust and mantle, seismic P-wave velocities and densities are compatible with quartzite in the upper crust, felsic granulite in the middle crust, mafic granulite in the lower crust and peridotite in the mantle. Furthermore, hydrated rheologies have been adopted for the continental crust and mantle, as these might be more appropriate for modelling purposes (Burov, 2003), particularly in continental environments affected by Post-Paleozoic tectono-thermal events (Afonso and Ranalli, 2004).

The rheology of the transitional region (TC) which is the addition of the OCT and part of Sub-domain 3B (Fig. 7A) is of crucial importance in this study. Its composition is difficult to represent since it contains stretched continental crust and either serpentinized mantle or intrude gabbros (Section 3.1). The brittle strength is however independent of composition, so we begin by considering the brittle part of the strength envelope (Fig. 7B).

Serpentinization in TC is suggested by localised deformation and a stretching factor larger than 3.0 (Fig. 2B). Models of extension at the West Iberia margin show that this stretching factor is consistent with embrittlement of the whole crust, with development of crustal penetrating faults acting as fluid conduits which allow serpentinization of the upper mantle peridotites (Pérez-Gussinyé and Reston, 2001). The coefficient of friction of serpentinite (~0.3) is considerably lower than that predicted by Byerlee's law (represented by the dashed line in Fig. 7B) being estimated that serpentinization can reduce the integrated strength of the lithosphere up to 30% (Escartín et al., 1997). Furthermore, serpentinites may favor the confinement of fluids within fault zones, contributing to a strength reduction of the whole lithosphere. We therefore tested a rheological weaker structure at the transitional zone where the brittle strength has been reduced in 30%.

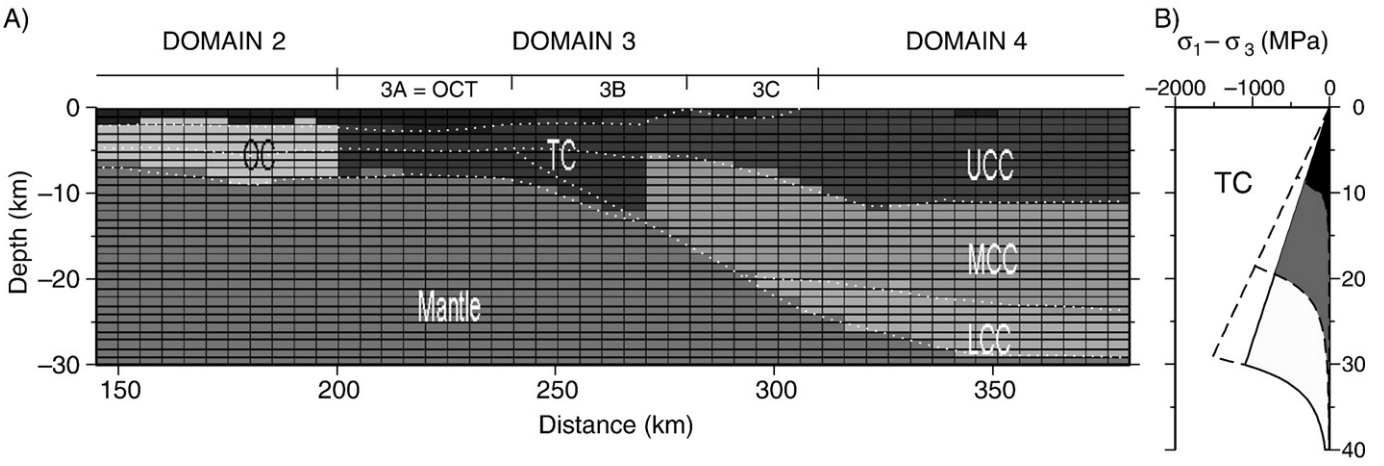

Fig. 7. A. Rheologies for the different layers are OC-dry diabase, UCC-wet quartzite, MCC-wet felsic granulite, LCC-wet mafic granulite, Mantle-wet peridotite. The transitional zone (TC) is a region of reduced brittle strength where several compositions were tested. B. Strength envelopes for the compositions tested in the transitional zone (TC) computed for geotherm GT3 (Fig. 6) and a strain rate of 10^{-16} s^{-1}. The dashed line corresponds to the standard Byerlee profile which has been reduced in 30%. The black envelope corresponds to wet quartzite (continental crust affinity), the grey envelope to wet diabase (oceanic crust affinity) and the white envelope to wet peridotite (mantle).

In contrast, the ductile part of the strength envelope, in particular the depth of the brittle–ductile transition for a particular geotherm, is controlled by composition (Fig. 7B). We considered three representative compositions in TC: a) wet quartzite, representing the behavior of a transitional zone with continental crust affinity; b) wet diabase, representing an intermediate behavior between continental and oceanic crust; c) wet peridotite, representing exhumed mantle. However, hypothesis c) is redundant in terms of modeling because the deformation regime within TC (which stands above ~8–15 km depth) is brittle for both wet peridotite and wet diabase (Fig. 7B).

The creep parameters for the several rheologies, as well as the heat production rates and thermal conductivities, were taken from Afonso and Ranalli (2004) and are listed in Table 1.

4.4. Modelling results

The most relevant features that resulted from the present modelling concern the evolution of the basin configuration, the distribution and evolution of the differential stress and the predicted pattern of failure.

4.4.1. Basin configuration

At the end of stage 2 we obtained the long-wavelength basin configuration due to the vertical loads shown in Fig. 8A. The modeled profile at this stage is compared with the Airy topography at the end of the Miocene, estimated by Airy backstripping the post-Miocene sediments along IAM-5. The good match between the modeled flexural profile and the filtered Airy topography for wavelengths larger than 100 km shows that the modelling procedure can adequately reproduce the long-wavelength configuration of the margin at the Miocene assuming isostatic equilibrium. As predicted by previous models of stress-induced vertical motions at extensional basins (e.g. Kooi and Cloetingth, 1992), the vertical loads are responsible for a downward state of flexure, characterized by concave upward flexure of the lithosphere beneath the largest sediment load.

Fig. 8B display the basin configuration at the beginning (black line) and at the end (grey line) of stage 3. Compression accentuates the downward flexure of the basin, producing uplift of the onshore and inner-shelf areas and dowanwarping of the outer shelf. For 2000 m of shortening (0.3% strain) the maximum uplift is ~500 m in the coastal plain, and the maximum subsidence is ~500 m in the center of the abyssal basin. As compression increases the shelf break migrates seaward and the continental slope becomes steeper (A → A′). At the western end of the basin, the location of zero net subsidence migrates landward (B → B′). The width of the abyssal basin remains approximately the same but its profile experiences differential vertical movements, i.e. the segment that corresponds to Domain 1 moves up and Domain 2 moves down.

4.4.2. Differential stress

The differential stress is the difference between the horizontal and vertical stress (σ_{xx}–σ_{zz}) in the vertical plane of the model. According to Anderson's theory of faulting (Anderson, 1951), normal faulting is associated with a state of stress in which the maximum compressive stress is the vertical stress and the minimum compressive stress is the horizontal stress. Thrust faulting is associated with a state of stress in which the horizontal stress is the maximum compressive stress. The

Table 1
Finite element model creep and thermophysical material parameters

	UCC (wet quartzite)	MCC (wet felsic granulite)	LCC (wet mafic granulite)	Sediments (wet quartzite)	OC (dry diabase)	TC (wet diabase)	Mantle (wet peridotite)
Q [μW m^{-3}]	1.4	0.4	0.4	1.2	–	1.4×10^{-6}	0.006
K [W m^{-1} K^{-1}]	2.5	2.1	2.1	2.3 (a)	–	2.1	3.0
ρ [kg m^{-3}]	2.6–2.7	2.74	3.0	2.3	2.62–2.97	2.62–2.97	3.3
A [MPa^{-n} s^{-1}]	3.2×10^{-4}	8.0×10^{-3}	1.4×10^{4}	3.2×10^{-4}	8.0	2.0×10^{-4}	2.0×10^{3}
B [kJ mol^{-1}]	154	243	445	154	485	260	471
n	2.3	3.1	4.2	2.3	4.7	3.4	4.0
E [Pa]	0.7×10^{11}	0.7×10^{11}	0.7×10^{11}	0.7×10^{11}	0.7×10^{11}	0.7×10^{11}	0.7×10^{11}
υ	0.25	0.25	0.25	0.25	0.25	0.25	0.25

Q — volumetric heat production rate; K — thermal conductivity; ρ — density; A,E,n — material creep parameters; E — Young's modulus; υ — Poisson's ratio. Both the power-law creep parameters as the thermal parameters are from Afonso and Ranalli (2004) except (a) which is from Fernandez et al. (1998).

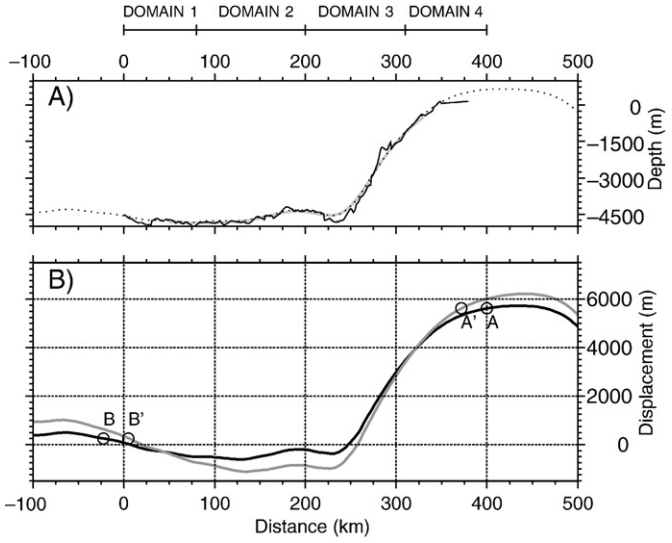

Fig. 8. A. Surface topography (top of the Miocene) predicted by the finite element model (dotted line) compared with surface topography estimated from Airy backstripping (solid black line). Grey solid line shows the backstripped topography filtered for wavelengths larger than 100 km. B. Predicted surface topography before (black line) and after (grey line) the application of 8 increments of 250 m of shortening. With compression, points A and B move inward of the basin to A′ and B′ respectively. The depocenter becomes deeper and the basin flanks are uplifted.

plane strain formulation implies the out-of-plane stress is the intermediate stress, so the models foresee a normal or thrust faulting regime depending on the sign and magnitude of the differential stress. We use the convention that negative differential stress is associated with a compressive faulting regime, and positive differential stress is associated with a normal faulting regime.

Stages 1 and 2 of modelling introduce a background state of stress prior to the onset of shortening (Fig. 9A). The time of relaxation is sufficiently long (500 increments of 50 years) to relax nearly all elastic stress above the yield strength envelope. Positive differential stresses corresponding to extension occur where the bending moment is positive and curvature is convex, at both ends of the model. The sediment load induces a compressive state of stress reaching a depth of about 30 km below seafloor, extending laterally from approximately km50 to km275. The maximum differential stress (~150 MPa) is negative and occurs in the region of maximum curvature, at the base of the continental slope.

Shortening in modelling stage 3 superimposes horizontal compressive stresses in the above stress pattern. As a result there is a gradual replacement of extension by compression in the upper levels at both ends of the sedimentary basin (Fig. 9B). Compressive differential stresses propagate downwards all the way along the profile.

At 2000 m of applied shortening no positive differential stresses remain in the model (Fig. 9C). Maximum compressive stresses (~420 MPa) occur in the transitional zone between km210 and km260, at approximately 6–7 km depth. At the oceanic end of the model, large compressive stresses (~250 MPa) concentrate in the upper mantle, where the brittle strength is largest. On the other end, the presence of large compressive stresses in the lower continental crust depends strongly on the assumed rheology. If a felsic instead of a mafic rheology was used, the stresses in the lower continental crust would be partially released because the yield strength would be reached and failure would occur.

4.4.3. Failure pattern

Failure is predicted where the differential stress exceeds the strength envelope. Failure above the brittle–ductile transition (Fig. 7B) is termed brittle while failure below this transition is termed ductile.

We are particularly interested in the deformation caused by Miocene shortening so we focus our attention to Fig. 10, which shows a close-up of the predicted pattern of failure for 2000 m of applied shortening. Two alternative compositions are considered in the transitional zone (TC): wet diabase (Fig. 10A) and wet quartzite (Fig. 10B). Both compositions produce a similar pattern of brittle failure, where 3 distinct regions are recognized: (1) to the west of the OCT, in Domain 2, brittle failure is observed up to a maximum depth of 3 km below the seafloor; (2) in Domain 3A and 3B, between km210 and km270, brittle failure extends from the surface to 5 km depth (Fig. 10A and B). This is consistent with the observation of faults cutting across both the sediments and the basement. Brittle failure in this region would not reach more than 3 km depth if the brittle strength in TC had not been reduced in 30%; (3) to the east of km270,

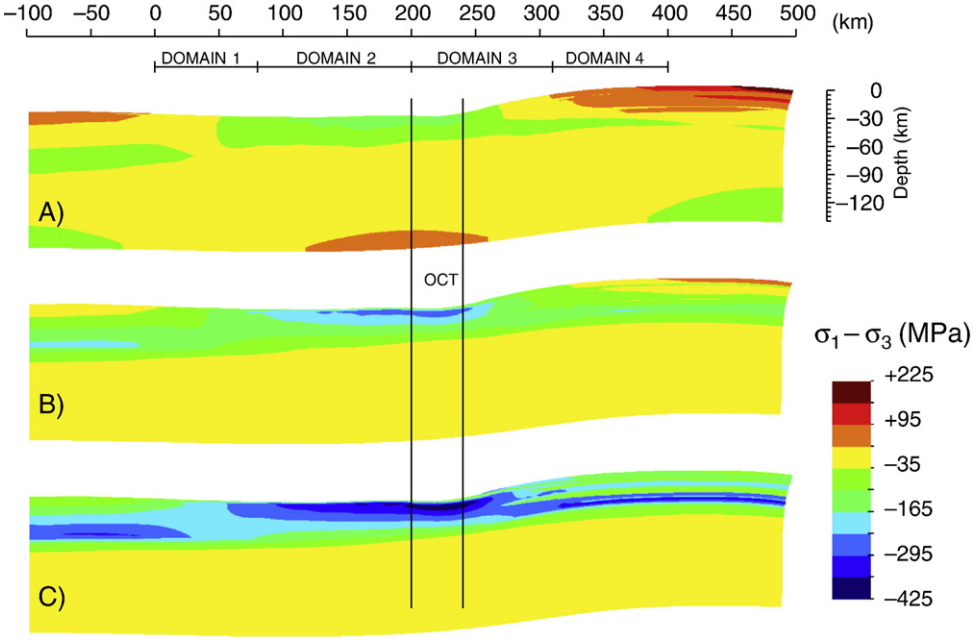

Fig. 9. Simulation of the response of the margin to Miocene shortening. Pattern of differential stress on a deformed frame (vertical deformation exaggeration factor ~4.5). A. Before the onset of shortening. B. After 1000 m of applied shortening. C. After 2000 m of applied shortening. Vertical lines mark the OCT limits.

in Domain 3C and Domain 4, brittle failure in compression is no longer observed at the surface. It sinks gradually remaining confined to a thin layer, 1–2 km thick, in the upper continental crust.

The main difference between Fig. 10A and B occurs in the pattern of ductile failure within the transitional zone (TC). While no ductile failure occurs for a transitional (wet diabase) composition (Fig. 10A), a continental rheology (wet quartzite) produces a region of ductile failure just underneath the region of brittle failure in compression (Fig. 10B). This allows for throughgoing failure of the crust in the transitional zone. In both cases (Fig. 10A and B) ductile failure is predicted to occur near the base of the upper continental crust (wet quartzite) at 7–11 km depth, near the base of the middle continental crust (felsic granulite) at 16–23 km depth and near the base of the lower continental crust (mafic granulite) at 27–30 km depth. These layers of ductile failure may act as decoupling regions.

5. Discussion

5.1. Reliability of the modeling results

Unlike other models of flexure at continental margins we do not take into account the depth of necking during rifting and the contribution of thermal contraction to subsidence and flexure (e.g. Braun and Beaumont, 1989; Weissel and Karner, 1989; Kooi and Cloetingth, 1992). However, our goal is not to study the rifting process or the details of the subsidence history of the basin, but the style of deformation that will develop in response to the Miocene shortening. The assumptions regarding the thermal structure and the rheological parameters also suffer from uncertainties and can be questioned. Nevertheless, these assumptions were extensively tested until the consistency between the modeling results and the large-scale geological observations gave us confidence in the approximations that were used.

5.2. Comparison of the modeling with observations

5.2.1. Basin configuration

Model predictions and geologic observations agree on the long-wavelength vertical differential motions induced by compression. In the oceanic realm stands out the contact between Domain 1 and Domain 2 (at km80, Fig. 5), which is associated to an abrupt landward crustal thickness reduction across an extensional fault. This fault may be related to the effect of Miocene shortening on the long-wavelength flexure of the margin, as it is consistent with predictions of Domain 1 moving up and Domain 2 moving down (Fig. 8B). At the contact between Domain 3B and Domain 3C stands out the normal fault FG bounding the halg-graben HG1 (at km280, Fig. 3), which accommodated most of the shortening. Immediately to the east the normal fault bounding the half-graben HG2 (Fig. 2) was only mildly inverted. While the location of these major normal faults near the contact between Domain 3 and Domain 4 concurs with subsidence of Domain 3 and uplift of Domain 4, the concentration of inversion in fault FG is consistent with the predicted downwarping of Domain 3B (Fig. 8B).

5.2.2. Differential stress

Even before the onset of shortening the numerical modelling predicts the concentration of maximum differential stresses at the base of the continental slope, between km190 and km250, as a result of maximum curvature and sediment loading. Latter shortening accommodation also concentrates in this region, thereby suggesting that fault reactivation is facilitated here because of the pre-existing high stress level (Fig. 9).

5.2.3. Failure pattern

Miocene and post-Miocene shortening structures did not develop within the abyssal basin, in Domain 2. This observation is not matched

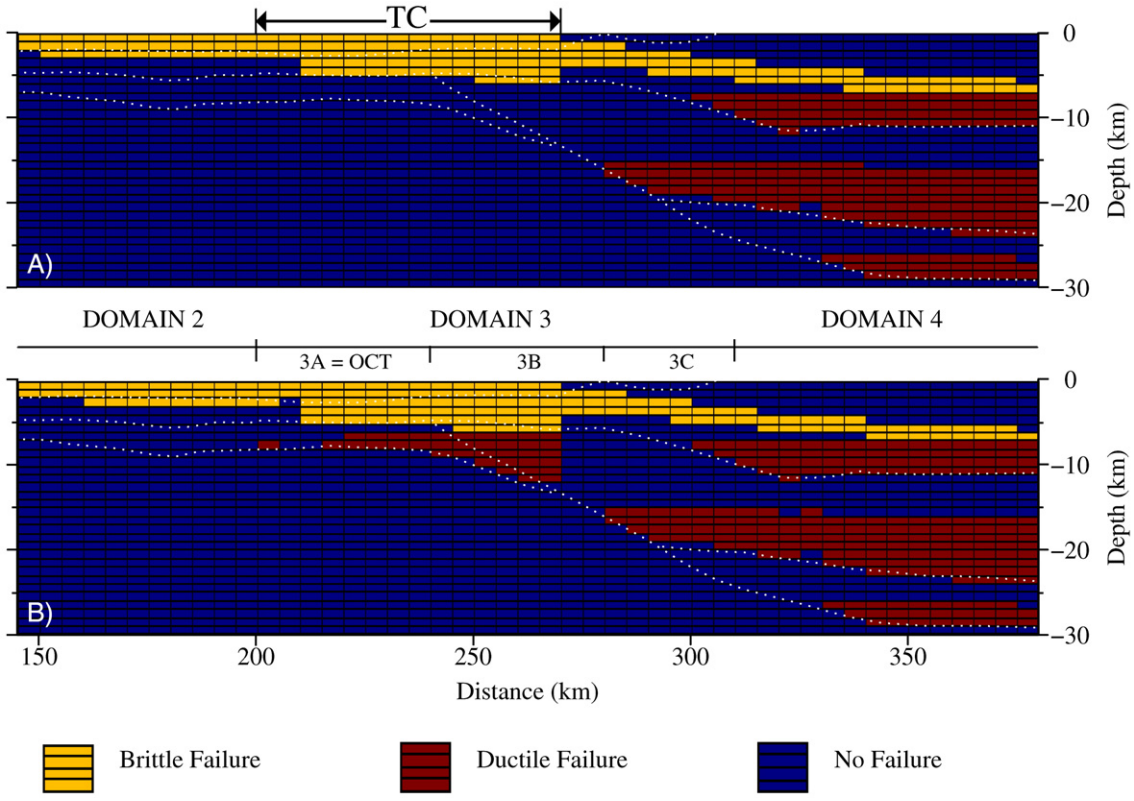

Fig. 10. Predicted pattern of failure on an undeformed frame for 2000 m of shortening. A. The transitional zone (TC) has a wet diabase composition to represent a region of intermediate strength between continental and oceanic crust. B. TC has a wet quartzite composition to represent a region of continental crust affinity. In any case brittle failure reaches the base of the upper crystalline crust in TC at ~5 km depth.

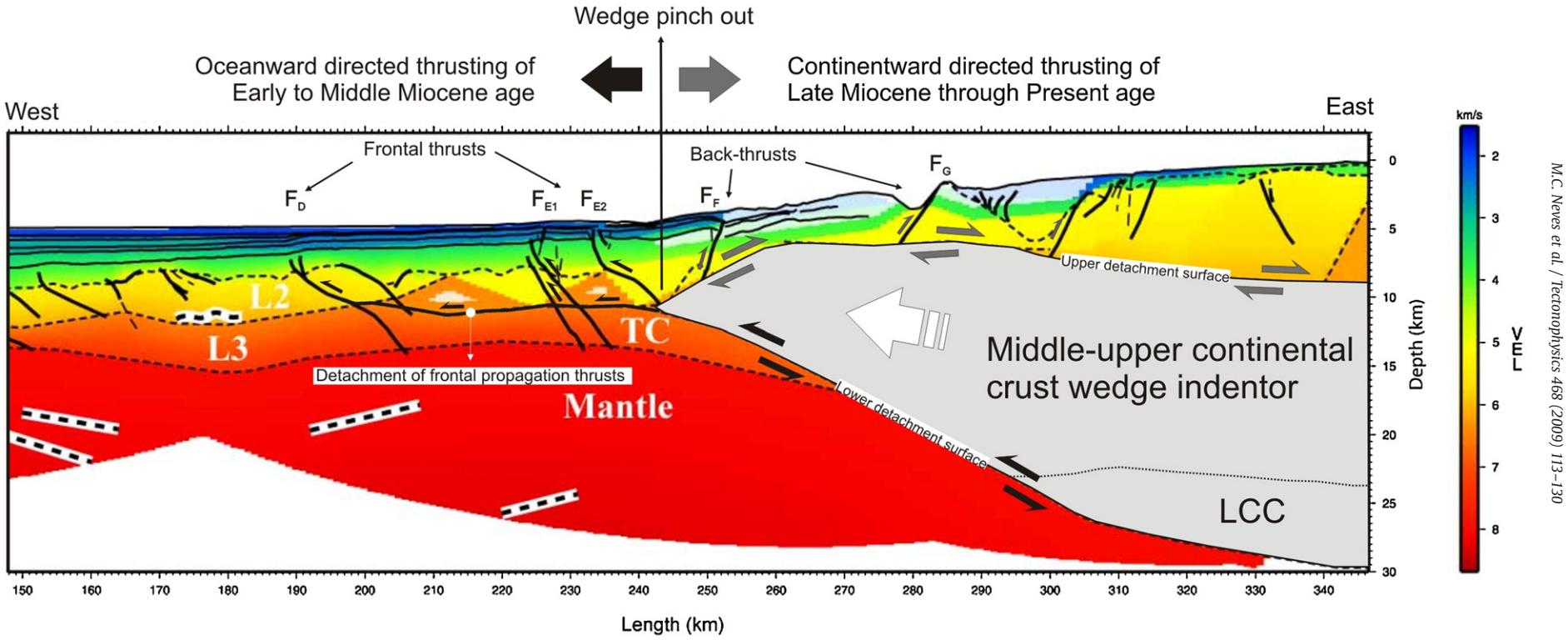

Fig. 11. Model for the propagation of the Miocene age deformation in the TAP by means of westwards directed indentation of a mid-upper continental wedge (white arrow). *Black arrows*: Initial oceanward directed thrusting during the Early through Middle Miocene; *Grey arrows*: continentward directed thrusting during the Late Miocene through Present.

by the numerical models, which predict that the differential stress exceeds the strength near the surface in Domain 2. This mismatch is possibly due to the zero cohesion assumption at the surface.

In the transitional zone the Miocene inversion was mainly accommodated by faults that reach at least ~5 km depth, such as F_{E2}, F_F and F_G (Figs. 2B, 3 and 11). The occurrence of brittle failure at these depths requires a 30% reduction of the brittle strength in TC relative to the surrounding regions. In addition to the faults mentioned several others are seen to extend across the lower crust and reach the Moho, particularly in the OCT, such as F_D and F_{E1} (Figs. 2B, 3 and 11). This evidence is not compatible with a continental rheology in the OCT because in this case the modeling predicts the occurrence of ductile failure in the lower crust, at depths greater than ~5 km (Fig. 10B). Ductile failure in the Miocene would be expected to erase the trace of any pre-existing faults at these depths. We therefore favor a transitional or serpentinized mantle composition in the lower crust in the OCT (Fig. 10A).

In contrast to the OCT, a continental rheology in the Sub-domain 3B at the level of the Middle Continental Crust (MCC) cannot be excluded. In fact, the MCC wedge in Sub-domain 3B is likely to have a similar rheology to the MCC layer in Sub-domain 3C (felsic granulite). According to Fig. 10B the pattern of ductile failure predicted for a continental composition would allow the basal boundary of the MCC wedge between approximately km240 and km300 to act as a decoupling zone. This would be consistent with the propagation model of the Miocene deformation we next describe.

5.3. The propagation of the Miocene deformation

The observations regarding the Miocene compression lead us to propose a model for the propagation of Miocene deformation in the TA. These observations are mainly:

i) the folding of sediments is associated to faulting and the best developed folds are located on the hanging-wall of reverse faults
ii) only minor deformation structures formed to the west of the abyssal basin, west of km80 in Domain 1
iii) FD, FE1 and FE2 (Fig. 3) are the only existent westwards directed reverse faults of Miocene age and they are located west of the mid-crust continental wedge
iv) to the east of the pinch-out of the mid-crust continental wedge (km245) thrusting is only eastwards directed
v) shortening initiated in the continental slope (east of km245) in Early to Middle Miocene times and propagated to the west when FD, FE1 and FE2 formed
vi) at the end of the Miocene FD, FE1 and FE2 ceased their activity and deformation has been accommodated since then to Recent times on the continental slope, i.e. east of the middle continental crust pinch-out, by means of eastwards directed thrusting
vii) the thick-skinned half-graben faults HG1 (Miocene through Present) and HG2 (Fig. 2A) (Miocene only) accommodated the eastwards directed thrusting.

The proposed model is schematically represented in Fig. 11. Its main characteristics are:

a) the mid and upper continental crust wedge between km240 and km280 controlled the location of the main shortening of Miocene age in the TAP, and consequently the basal boundary of the mid-continental crust between km240 and km300 played the role of upthrusting ramp propagating deformation in the underlying transitional crust detaching on top of the Moho. This hypothesis is supported by the numerical modelling.
b) the top of the basement-base of the rift basin acted as a detachment horizon to the eastwards directed thrusting of Pliocene through Present times.
c) the mid-continental crust and the upper continental crust wedge acted as a flake-type indenter propagating divergent diachronous thrusting: westwards directed thrusting (oceanwards) in the transitional crust (eastern part of Domain 2 and Sub-domain 3A) during Late Miocen and possibly Early Pliocene, and eastwards on the top of the basement and basin in the continental slope during the Pliocene through Present.
d) the half-grabens (HG1 and HG2) extensional faults acted as a buttresses to the eastward propagation of deformation

6. Conclusion

Tectonic deformation associated with the Miocene and post-Miocene compressive events, with NW–SE and WNW–ESE oriented main horizontal compression directions, was accommodated in Domain 1 and especially in the transitional region TC which includes the OCT and an adjacent continental segment. In Domain 1 inversion was accommodated only by wrenching on oceanic extensional faults adjacent to the TMR lithosphere. In the OCT and continental slope, it was mainly accommodated on inverted rift faults, trending NE–SW and N–S, and tectonic vergence was directed both towards the ocean in the Miocene and towards the continent in the Pliocene–Quaternary.

The concentration of deformation in the transitional zone requires unusual constitutive laws in the brittle regime. To explain the observed accommodation of Miocene shortening the frictional strength in the TC needs to be reduced by ~30% when compared with surrounding regions. The choice of a continental or oceanic composition in TC has only implications on the existence of a region of ductile failure beneath ~5 km depth. While a stronger rheology precludes the existence of whole crust failure, a more continental-like composition is consistent with flow of the lower crust. To the west of km240, in the OCT, the clear evidence of faults below 5 km depth is not consistent with ductile flow and therefore the modeling supports a transitional or serpentinized mantle composition in this region. In contrast, to the east of km240 a continental composition is consistent with the existence of a decoupling zone at the base of the mid-continental crust. This supports the hypothesis of a mid-continental crust–upper continental crust wedge that acted as an indenter controlling the location of the Miocene deformation in the TAP. According to this hypothesis oceanwards directed thrusting lies at the tip of this wedge and continentwards directed thrusting ramps up on top of a decollement at the basement–rift basin interface, probably the evaporites of Late Triassic–earliest Jurassic age.

Acknowledgements

The authors and the Instituto Nacional de Engenharia, Tecnologia e Inovação (INETI) acknowledge the support by Landmark Graphics Corporation via the Landmark University Grant Program. M. Moulin is sponsored by LATTEX/IDL grant — ISLF-5-32 cofinanced by FEDER. We thank C. Pascal and an anonymous reviewer for very helpful comments.

References

Anderson, E.M., 1951. The Dynamics of Faulting and Dyke Formation with Applications to Britain. Oliver and Boyd, Edinburgh. 206 pp.
Afilhado, A., Matias, L., Shiobara, H., Hirn, A., Mendes-Victor, L., Shimamura, H., in press. From unthinned continent to ocean: the deep structure of the West Iberia passive continental margin at 38°N. Tectonophysics.
Afonso, J.C., Ranalli, G., 2004. Crustal and mantle strengths in continental lithosphere: is the jelly sandwich model obsolete? Tectonophysics 394, 221–232.
Alves, T.M., Gawthorpe, R.L., Hunt, D.W., Monteiro, J.H., 2003. Cenozoic tectono-sedimentary evolution of the western Iberian margin. Mar. Geol. 195, 75–108.
Auzende, J.M., Olivet, J.-L., Charvet, J., Le Lann, A., Le Pichon, X., Monteiro, J.H., Nicolas, A., Ribeiro, A., 1978. Sampling and observation of the oceanic mantle and crust on Gorringe Bank. Nature 273, 45–48.
Banda, E., Torné, M., IAM group, 1995. IAM group investigates deep structure of ocean margins. EOS Trans. 76, 25–29.

Boillot, G., Winterer, E.L., Meyer, A.W., et al. (Eds.), 1987. Proceedings of the Ocean Drilling Program, Initial Reports, 103. Ocean Drilling Program, College Station, TX.
Boillot, G., Feraud, G., Recq, M., Girardeau, J., 1989. Undercrusting by serpentinite beneath rifting margins. Nature 341, 523–525.
Bott, M.H.P., 1997. Modeling the formation of a half graben using realistic upper crustal rheology. J. Geophys. Res. 102, 24605–24617.
Bott, M.H.P., 1999. Modeling local crustal isostasy caused by ductile flow in thelower crust. J. Geophys. Res. 104, 20349–20359.
Braun, J., Beaumont, C., 1989. A physical explanation of the relationship between flank uplifts and the breakup unconformity at rifted continental margins. Geology 17, 760–764.
Buforn, E., Bezzeghoud, M., Udias, A., Pro, C., 2004. Seismic sources in the Iberian–African plate boundary and their tectonic implications. Pure Appl. Geophys. 161 (3), 623–646.
Burov, E.B., 2003. The upper crust is softer than dry quartzite. Tectonophysics 361, 321–326.
Chian, D.P., Louden, K.E., Minshull, T.A., Whitmarsh, R.B., 1999. Deep structure of the ocean–continent transition in the southern Iberia Abyssal Plain from seismic refraction profiles: Ocean Drilling Program (Legs 149 and 173) transect. J. Geophys. Res. 104, 7443–7462.
Christensen, N.I., Mooney, W.D., 1995. Seismic velocity structure and composition of the continental crust: a global view. J. Geophys. Res. 100, 9761–9788.
Contrucci, I., Klingelhoefer, F., Perrot, J., Bartolome, R., Gutscher, M.-A., Sahabi, M., Malod, J.P., Rehault, J.-P., 2004. The crustal structure of the NW-Moroccan continental margin from wide-angle and reflection seismic data. Geophys. J. Int. 159, 117–128.
Dean, S.M., Minshull, T.A., Whitmarsh, R.B., Louden, K.E., 2000. Deep structure of the ocean–continent transition in the southern Iberia Abyssal Plain from seismic refraction profiles: the IAM-9 transect at 40 degrees 20′N. J. Geophys. Res. 105, 5859–5885.
Escartín, J., Hirth, G., Evans, B., 1997. Effects of serpentinization on the lithospheric strength and the style of normal faulting at slow-spreading ridges. Earth Planet. Sci. Lett. 151 (3–4), 181–190.
Fernandez, M., Marzán, I., Correia, A., Ramalho, E., 1998. Heat flow, heat production, and lithospheric thermal regime in the Iberian Peninsula. Tectonophysics 291, 29–53.
Fernandez, M., Marzán, I., Torné, M., 2004. Lithospheric transition from the Variscan Iberian Massif to the Jurassic oceanic crust of the Central Atlantic. Tectonophysics 386, 97–115.
Funck, T., Hopper, J.R., Larsen, H.C., Louden, K.E., Tucholke, B.E., Holbrook, W.S., 2003. Crustal structure of the ocean–continent transition at Flemish Cap: seismic refraction results. J. Geophys. Res. 108, 2531. doi:10.1029/2003JB002434.
Gonzalez, A., Cordoba, D., Vales, D., 1999. Seismic crustal structure of Galicia continental margin, NW Iberian Peninsula. Geophys. Res. Lett. 26 (8), 1061–1064.
Hopper, J.R., Funck, T., Tucholke, B.E., Louden, K.E., Holbrook, W.S., Larsen, H.C., 2004. Continental breakup and the onset of ultraslow seafloor spreading off Flemish Cap on the Newfoundland rifted margin. Geology 32 (1), 93–96.
Hopper, J.R., Funck, T., Tucholke, B.E., Louden, K.E., Holbrook, W.S., Larsen, H.C., 2006. A deep seismic investigation of the Flemish Cap margin: implications for the origin of deep reflectivity and evidence for asymmetric break-up between Newfoundland and Iberia. Geophys. J. Int. 164 (3), 501–515.
Jiménez-Munt, M., Fernandez, M., Torné, M., Bird, P., 2001. The transition from linear to diffuse plate boundary in the Azores–Gibraltar region: results from a thin sheet model. Earth Planet. Sci. Lett. 192, 175–189.
Kelemen, P.B., Holbrook, W.S., 1995. Origin of thick, high-velocity igneous crust along the US east-coast margin. J. Geophys. Res. 100, 10077–10094.
Klitgord, K.D., Schouten, H., 1986. Plate kinematics of the central Atlantic. In: Vogt, P.R., Tucholke, N.E. (Eds.), The Geology of the North Atlantic. Geol. Soc. Am., vol. M. The Western North Atlantic Region, pp. 351–378.
Kooi, H., Cloetingth, S., 1992. Lithospheric necking and regional isostasy at extensional basins 2. Stress-induced vertical motions and relative sea level changes. J. Geophys. Res. 97, 17573–17591.
Kullberg, M.C., Kullberg, J.C., Terrinha, P., 2000. Tectónica da cadeia da Arrábida, Tectónica das regiões de Sintra e Arrábida. Mem. Geociênc., Museu Nac. Hist. Nat. Univ. Lisboa 2, 35–84.
Kullberg, J.C., Terrinha, P., Pais, J., Reis, R.P., Legoinha, P., 2006. Arrabida e Sintra: dois exemplos de tectónica post rifting da Bacia Lusitaniana. In: Dias, R., Araújo, A., Terrinha, P., Kullberg, J.C. (Eds.), Geologia de Portugal no contexto da Ibéria. Univ. Évora, pp. 369–395.
Lau, K.W.H., Louden, K.E., Funck, T., Tucholke, B.E., Holbrook, W.S., Hopper, J.R., Larsen, H.C., 2006a. Crustal structure across the Grand Banks–Newfoundland Basin continental margin — I. Results from a seismic refraction profile. Geophys. J. Int. 167, 127–156.
Lau, K.W.H., Louden, K.E., Funck, T., Tucholke, B.E., Holbrook, W.S., Hopper, J.R., Larsen, H.C., 2006b. Crustal structure across the Grand Banks–Newfoundland Basin continental margin — II. Results from a seismic reflection profile. Geophys. J. Int. 167, 157–170.
Masson, D.G., Cartwright, J.A., Pinheiro, L.M., Whitmarsh, R.B., Beslier, M.O., Roeser, H., 1994. Compressional deformation at the ocean–continent transition in the NE Atlantic. J. Geol. Soc. Lond. 151, 607–613.
Mauffret, A., Mougenot, D., Miles, P.R., Malod, J.A., 1989. Cenozoic deformation and Mesozoic Abandoned Spreading Center in the Tagus Abyssal-Plain (West of Portugal) — results of a Multichannel Seismic Survey. Can. J. Earth Sci. 26 (6), 1101–1123.
Miles, P.R., Verhoef, J., Macnab, R., 1996. Compilation of magnetic anomaly chart west of Iberia. Seismic stratigraphy and tectonic history of the Iberia Abyssal Plain. In: Whitmarsh, R.B., Sawyer, D.S., Klaus, A., Masson, D.G. (Eds.), Proc. ODP, Sci. Results, 149. Ocean Drilling Program, College Station, TX, pp. 659–663.
Minshull, T.M., Dean, S.M., Whitmarsh, S.B., Russell, S.M., Louden, K.E., Chian, D., 1998. Deep structure in the vicinity of the ocean–continent transition zone under the southern Iberia abyssal plain. Geology 26, 743–746.
Negredo, A.M., Bird, P., Sanz de Galdeano, C., Buforn, E., 2002. Neotectonic modeling of the Ibero–Maghrebian region. J. Geophys. Res. 107, 2292. doi:10.1029/2001JB000743.
Neves, M.C., Neves, R.G.M., submitted for publication. Flexure and seismicity across the ocean–continent transition in the Gulf of Cadiz. Journal of Geodynamics.
Neves, M.C., Bott, M.H.P., Searle, R.C., 2004. Patterns of stress at midocean ridges and their offsets due to seafloor subsidence. Tectonophysics 386 (3–4), 223–242.
Okaya, N., Freeman, R., Kissling, E., Mueller, St., 1996. A lithospheric cross-section through the Swiss-Alps: II. Constraints on the mechanical structure of a continent–continent collision. Geophys. J. Int. 127, 399–414.
Olivet, J.L., 1996. Kinematics of the Iberian Plate. Bull. Centres de Recherches Exploration-Production Elf Aquitaine 20, 131–195.
Owen, D.R.J., Hinton, E., 1980. Finite Elements in Plasticity: Theory and Practice. Pineridge Press Ltd. 594 pp.
Pérez-Gussinyé, M., Reston, T.J., 2001. Rheological evolution during extension at passive non-volcanic margins: onset of serpentinization and development of detachments leading to continental break-up. J. Geophys. Res. 106, 3961–3975.
Pickup, S.L.B., Whitmarsh, R.B., Fowler, C.M.R., Reston, T.J., 1996. Insight into the nature of the ocean–continent transition of West Iberia from a deep multichannel seismic reflection profile. Geology 24, 1079–1082.
Pinheiro, L.M., Whitmarsh, R.B., Miles, P.R., 1992. The ocean continent boundary off the western continental-margin of Iberia 2. Crustal structure in the Tagus Abyssal-Plain. Geophys. J. Int. 109 (1), 106–124.
Pinheiro, L.M., 1994. The crustal structure under the Tagus abyssal plain and the ocean continent transition off western Iberia. PhD Thesis, Imperial College, London, 381 pp.
Ranalli, G., 1995. Rheology of the Earth, 2nd ed. Chapman & Hall, London. 413 pp.
Reid, I.D., 1994. Crustal structure of a nonvolcanic rifted margin east of Newfoundland. J. Geophys. Res. 99, 15161–15180.
Reston, T.J., Krawczyk, C.M., Klaeschen, D., 1996. The S reflector west of Galicia (Spain): evidence from prestack depth migration for detachment faulting during continental breakup. J. Geophys. Res. 101, 8075–8091.
Ribeiro, A., Kullberg, M.C., Kullberg, J.C., Manuppella, G., Phipps, S., 1990. A review of Alpine Tectonics in Portugal: foreland detachment in basement and cover rocks. Tectonophysics 184, 357–366.
Roque, C., 2007. Tectonostratigafia das margens continentais sul e sudoeste portuguesas: um modelo de correlação sismostratigráfica. PhD. Thesis, Faculdade de Ciências de Lisboa, Univ. de Lisboa, 310 pp.
Rovere, M., Ranero, C.R., Sartori, R., Torelli, L., Zitellini, N., 2004. Seismic images and magnetic signature of the Late Jurassic to Early Cretaceous Africa–Eurasia plate boundary off SW Iberia. Geophys. J. Int. 158 (2), 554–568.
Ryan, W.B.F., Hsü, K.J., Cita, M.B., Dumitrica, P., Lort, J.M., Maync, W., Nesteroff, W.D., Pautot, G., Stradner, H., Wezel, F.C., 1973. Site DSDP 120. Initial Reports of the DSDP 13, 19–41.
Sartori, R., Torelli, L., Zitellini, N., Peis, D., Lodolo, E., 1994. Eastern segment of the Azores-Gibraltar line (central-eastern Atlantic): an oceanic plate boundary with diffuse compressional deformation. Geology 22, 555–558.
Sawyer, D.S., 1994. The case for slow-spreading oceanic crust landward of the peridotite ridge in the Iberia Abyssal Plain. Eos 75, 616 (Abstract).
Sawyer, D.S., Whitmarsh, R.B., Klaus, A., et al., 1994. Proceedings of the Ocean Drilling Program, Initial Reports, 149. Ocean Drilling Program, College Station, TX.
Sibson, R.H., 1974. Frictional constraints on thrust, wrench and normal faults. Nature 249, 542–544.
Sibuet, J.-C., Srivastava, S.P., Spakman, W., 2004. Pyrenean orogeny and plate kinematics. J. Geophys. Res. 109. doi:10.1029/2003JB002514.
Sibuet, J.C., Srivastava, S., Manatschal, G., 2007. Exhumed mantle-forming transitional crust in the Newfoundland–Iberia rift and associated magnetic anomalies. J. Geophys. Res. 112, B06105. doi:10.1029/2005JB003856.
Shillington, D.J., Holbrook, W.S., Van Avendonk, H.J.A., Tucholke, B.E., Hopper, J.R., Louden, K.E., Larsen, H.C., Nunes, G.T., 2006. Evidence for asymmetric nonvolcanic rifting and slow incipient oceanic accretion from seismic reflection data on the Newfoundland margin. J. Geophys. Res. 111, B09402. doi:10.1029/2005JB003981.
Srivastava, S.P., Sibuet, J.-C., Cande, S., Roest, W.R., Reid, I.D., 2000. Magnetic evidence for slow seafloor spreading during the formation of the Newfoundland and Iberian margins. Earth Planet. Sci. Lett. 182, 61–76.
Terrinha, P., 1998. Structural geology and tectonic evolution of the Algarve Basin, South Portugal, PhD Thesis, Imperial College of Science, Technology and Medicine, Univ. of London, 425 pp.
Terrinha, P., Matias, L., Vicente, J.C., Duarte, J., Luís, J., Pinheiro, L., Lourenço, N., Diez, S., Rosas, F.M., Magalhães, V., Valadares, V., Zitellini, N., Mendes-Víctor, L., MATESPRO Team, submitted for publication. Morphotectonics and strain partitioning at the Iberia–Africa plate boundary from multibeam and seismic reflection data. Marine Geology.
Tucholke, B.E., Sibuet, J.-C., Klaus, A., et al. (Eds.), 2004. Proceedings of the Ocean Drilling Program, Initial Reports, 210. Ocean Drilling Program, College Station, TX.
Turcotte, D.L., Schubert, G., 2002. Geodynamics. Cambridge University Press. 441 pp.
Van Avendonk, H.J.A., Holbrook, W.S., Nunes, G.T., Shillington, D.J., Tucholke, B.E., Louden, K.E., Larsen, H.C., Hopper, J.R., 2006. Seismic velocity structure of the rifted margin of the eastern Grand Banks of Newfoundland. Can. J. Geophys. Res. 111. doi:10.1029/2005JB004156.
Verhoef, J., Roest, W.R., Macnab, R., Arkani-Hamed, J., Project Team, 1996. Magnetic anomalies of the Arctic and North Atlantic Oceans and Adjacent land areas. GSC Open file 3125. Geological Survey of Canada, p. 225.
Weissel, J., Karner, G., 1989. Flexural uplift of rift flanks due to mechanical unloading of the lithosphere during extension. J. Geophys. Res. 94. doi:10.1029/89JB01075.
White, R.S., McKenzie, D.P., 1989. Magmatism at rift zones: the generation of volcanic continental margins and flood basalts. J. Geophys. Res. 94, 7685–7729.
Whitmarsh, R.B., Miles, P.R., 1995. Models of the development of West Iberia rifted continental margin at 40 degrees 30′ N deduced from surface and deep-tow magnetic anomalies. J. Geophys. Res. 100, 3789–3806.

Whitmarsh, R.B., Miles, P.R., Mauffret, A., 1990. The ocean–continent boundary off the western continental margin of Iberia I. Crustal Structure at 40°30′N. Geophys. J. Int. 103, 509–531.

Whitmarsh, R.B., White, R.S., Horsefield, S.J., Sibuet, J.-C., Recq, M., Louvel, V., 1996. The ocean–continent boundary off the western continental margin of Iberia: crustal structure west of Galicia Bank. J. Geophys. Res. 101, 28291–28314.

Whitmarsh, R.B., Beslier, M.-O., Wallace, P.J., et al. (Eds.), 1998. Proceedings of the Ocean Drilling Program, Initial Reports, 173. Ocean Drilling Program, College Station, TX.

Whitmarsh, R.B., Manatschal, G., Minshull, T.A., 2001. Evolution of magma-poor continental margins from rifting to seafloor spreading. Nature 413, 150–154.

Wilson, R.C.L., Sawyer, D.S., Whitmarsh, R.B., Zerong, J., Carbonell, J., 1996. Seismic stratigraphy and tectonic history of the Iberia Abyssal Plain. In: Whitmarsh, R.B., Sawyer, D.S., Klaus, A., Masson, D.G. (Eds.), Proc. ODP, Sci. Results, 149. Ocean Drilling Program, College Station, TX, pp. 617–633.

Zhang, G.B., Bott, M.H.P., 2000. Modelling the evolution of asymmetrical basins bounded by high-angle reverse faults with application to foreland basins. Tectonophysics, 322 (3), 203–218.

Zitellini, N., Mendes, L.A., Cordoba, D., Danobeitia, J., Nicolich, R., Pellis, G., Ribeiro, A., Sartori, R., Torelli, L., Bartolomé, R., Bortoluzzi, G., Calafato, A., Carrilho, F., Casoni, L., Chierici, F., Corela, C., Correggiari, A., Della Vedova, B., Gràcia, E., Jornet, P., Landuzzi, M., Ligi, M., Magagnoli, A., Marozzi, G., Matias, L., Penitenti, D., Rodriguez, P., Rovere, M., Terrinha, P., Vigliotti, L., Zahinos Ruiz, A., 2001. Source of 1755 Lisbon Earthquake and Tsunami Investigated. EOS Trans. 82, 290–291.

Zitellini, N., Matias, L., Rovere, M., Voltaire team. Voltaire, 2002. Cruise report, Consiglio Nazionale delle Ricerche, Bologna. IGMCNR. Tech. Rep. 79, 33.

Zitellini, N., Rovere, M., Terrinha, P., Chierici, F., Matias, L., BIGSETS Team, 2004. Neogene through Quaternary tectonic reactivation of SW Iberian passive margin. Pure App. Geophys. 161 (3), 565–587.